2.1 INTRODUCTION :

The usefulness of ferrites is determined by their physical and chemical properties which fall in the two categories, one being intrinsic to the constitution of ferrites and the other extrinsic i.e. structure sensitive. To the extent, the method of preparation needs heat treatment for the formation of the crystal structure, and it also influences the intrinsic properties which are usually understood in terms of cation distribution. However, the details of the heat treatment like firing temperature, time, atmosphere, and cooling rate etc. cumulatively constitute the thermal history of the sample, through the imprint on almost all the attendant microstructural factors like defect concentration, porosity, inclusions and orientation, size and shape of the grains. Further in the method of preparation due care has to be taken into consideration regarding the homogeneity of the material, so that chemical composition and phase relationship are not adversely affected by the disproportionate non-equillibrium component of the heat treatment.

The ceramic method makes it possible to prepare complex chemical composition, desired microstructures and shapes of the final product much more economically than the single crystals. Ceramics provides a way of avoiding undesired effects such as eddy current losses which can be suppressed by internal lamination along grain boundries.[1]

In this chapter a brief review of the method of preparation, ceramic processes and development of microstructure relating to time and temperature are discussed. Role of atmosphere which influences the microstructure of ferrites is also discussed. The method of preparation of ferrite samples in the laboratory is briefly dealt with.

SECTION - A

2.2 PREPARATION OF FERRITES :

Ferrites being the oxidematerials no special extraction or preparation techniques involving molten phases are required. In the preparation, the starting materials are allowed to undergo solid state reaction and therefore, it is usually called ceramic process. Basically there are four steps in the preparation of ferrite materials for required applications. A flow chart is given in Fig. 2.1.

(1) Preparation of material to form an intimate mixture with the metal ions in the ratio which they will have in the final product.

(2) Heating of this mixture to form the ferrite (often called as pre-sintering).

(3) Powdering of pre-sintered material and pressing or forming the required shape.

(4) Sintering to form the final product.

These four steps may not be of distinct in nature but they can be varied with the requirement.

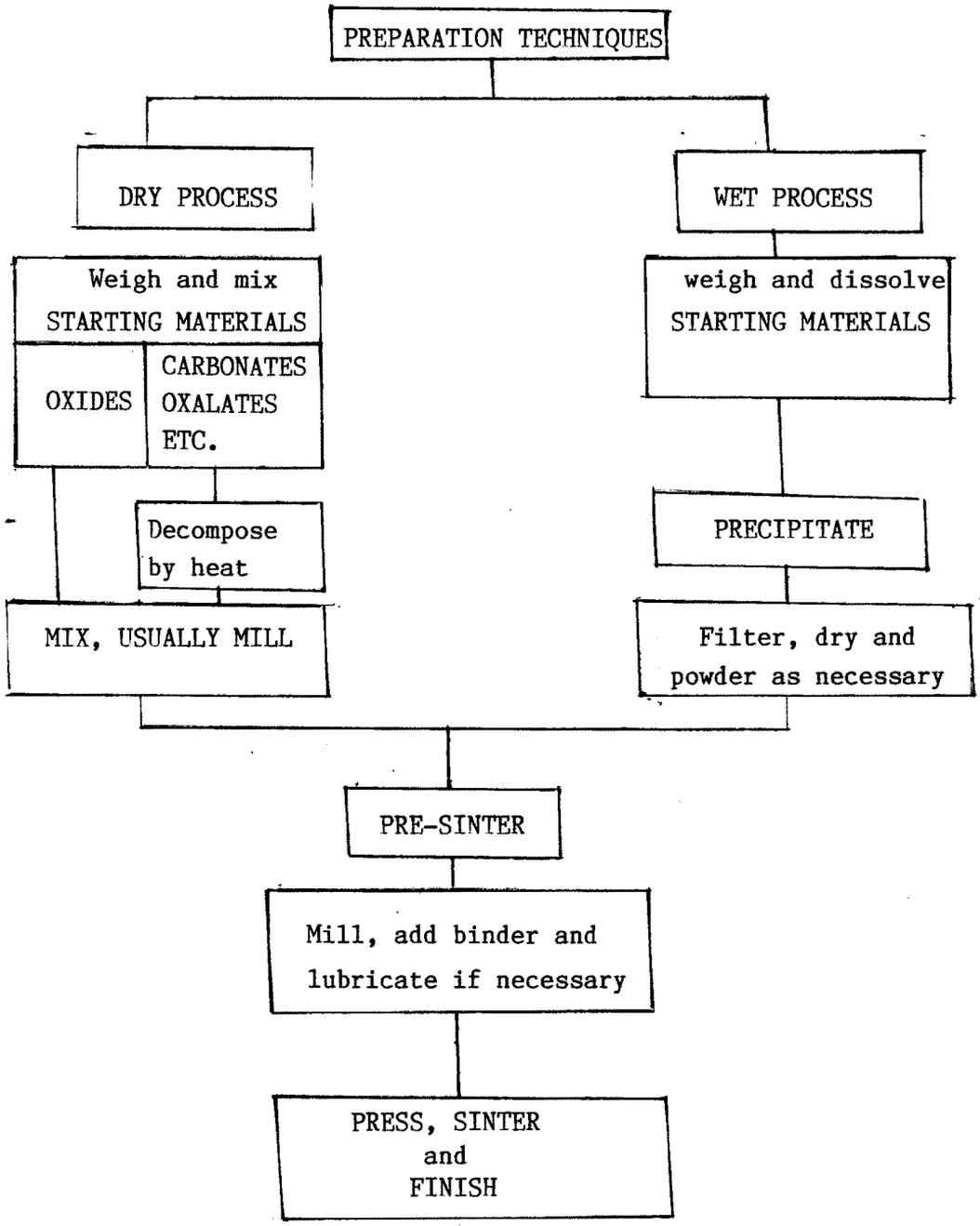

Fig. 2.1 Flow chart of the stages in ferrite preparation.

2.3 PREPARATION OF FERRITE COMPOSITION :

The general methods for preparation of ferrite composition are given as follows,

(a) Oxide method

(b) Decomposition method

(c) Hydroxide precipitation

(d) Oxalate precipitation

2.3(a) Oxide Method :

This method is most extensively used in the commercial production of ferrites, which requires little chemical knowledge. High purity oxides of materials in required proportion for final product are mixed together. One can mix carbonates with iron oxide. They are mixed manually and wet milled with steel-balls for few hours. After milling mixture is dried, then the powder is passed through the mesh screen. The mixture is calcined at elevated temperature and powdered and dried. Then pressed it into suitable shape and finally sintered.

The other mixing methods are discussed elsewhere[2].

2.4 SINTERING :

Sintering is a process where the material is forced in equilli brium concentration and develops the final microstructure. There are two steps of sintering.

(a) Pre-sintering

(b) Final sintering.

2.4(a) Pre-sintering :

The purpose of pre-sintering is to decompose higher oxides and carbonates which reduces the evolution of gas in the final sintering process. Secondly it assists in homogenizing of the material and also to reduce variation in the compositions of raw material Lastly it is necessary to control the shrinkage of the material which occur during final sintering. During pre-sintering the raw materials partly react to form final product and an amount of reaction depends on the reactivity of the components and on pre-sintering temperature.[3]

2.4(b) Final Sintering :

The final microstructure develops during this sintering process. We assume that the cations are present in correct proportions. The object then remains to achieve a suitable microstructure together with correct oxygen content and the distribution of cations. These are affected by the time and temperature of sintering. The partial pressure of oxygen or any other sintering atmosphere and cooling rate. Perdujin and Peloshek[8] have commented, "A quantitative study of the contribution of each parameter to the magnetic properties should take years of work or be perhaps impossible. However, by qualitative considerations good results can be obtained and improvement can be achieved."

Sintering consists of heating the compact to a temperature at which the mobility is sufficient to permit the decrease of free energy associated with grain boundaries. Extensive reviews on grain

growth and sintering are available.[4,5] During sintering densification and grain growth occur at the same time and give rise to a variety of microstructures. Sintering reactivity is important for densification. This reactivity is defined as the amount of energy available for sintering must be sufficiently high for the process to proceed i.e. the particle size of the powder must be small. Surface energy is defined by an equation

$$E = \frac{\sigma r}{D} \qquad \ldots (2.1)$$

Where r = surface tension

D = diameter of spherical powder

As sintering and densification requires material to be transported, it is equally important that material possesses good sinterability. Volume diffusion is main transport mechanism in ionic solids such as spinels. Surface diffusion may play a part in the beginning of the process in the formation of contact area between particles. Before the start the powder is compacted in such a way that density is high to have good contact between particles.[5] Nabarrao[6] Heiring[7] theory for diffusional microcreep is considered to be principal mecha nism for densification. The surface of the pore act as source of vacancies. These vacancies diffuse through the bulk of the particles to the grain boundries, where they can be discharged. The resulting effect is material transport by the migration of individual ions from the grain boundries to the pores producing shrinkage.

Migration of vacancies occur as a result of concentration gradient between the curved surface of the pores and equillibrium vacancy concentration under the flat surface C_o. The vacancy concen-

tration (C_r) under the surface of radius of curvature r is given by Kelvine equation,

$$C_{(r)} = C_o \exp \frac{(2r_s a^3)}{r.KT} \quad \ldots (2.2)$$

a^3 = vacancy volume.

As the concentration of grain boundry is assumed to be equal to C_o and vacancy migrate at temperature where the mobility is sufficiently high from the pore surface to the grain boundries. In grain growth the grain boundry energy is decreased when the boundries move to their center of curvature. Topology requires that in two dimensional picture grains with more than six sides have boundries with concave curvature. For large grains usually have more sides than those of smaller grains. Former grows at the expense of the later. The rate of grain growth is given[8]

$$D - D_o = Kt^n \quad \ldots (2.3)$$

where,

D_o = original particle size

K = temperature dependent factor

t = time

The expected rate of grain growth is proportional to $t^{\frac{1}{2}}$, however in practice the lower rate of grain growth is observed which is proportional to $t^{1/3}$ due to the presence of impurities and inclusions in the grain boundries. Grain growth during sintering is almost impossible to describe in general terms and also difficult to control in practice. Zener[9] has given a purely empirical relationship for discontinuous grain growth.

$$D_{cr} = \frac{di}{fi} \quad D_c < \frac{4D}{3f} \qquad \ldots (2.4)$$

di = diameter of inclusion

fi = fraction volume

When grain size has reached this dimension further grain growth is inhibited. In this situation a larger grain is formed, it can grow very rapidly to a much larger size than the matrix.

Lack of chemical homogeneity as well as variations in density and the presence of impurities can influence discontinuous grain growth. If the initial powder is incompletely reacted there is a volume change as the ferrite is formed at sintering temperature leading to porosity and stresses that may result possibly in cracking.[10]

2.4 (c) Sintering Atmosphere

It has been observed that sintering atmosphere plays an important role in sintering process. It must be remembered that Fe_2O_3 content can depend on the degree of oxidation or reduction of ferrite It can result of varying the MO/Fe_2O_3 ratio of the ferrite. Deficiency of Fe_2O_3 appears to lead to the highest eventual density for Ni-Zn ferrite but introduce second phase inclusions. It is fortunate that with second phase inclusions, it is possible to achieve 100% density at or very near to stoichiomatric composition.[11] The reduction of ferric to ferrous ion occurs at high temperature or at low oxygen pressure.[12] The explanation for an effect of deficit Fe_2O_3 was given by Reignen[12]. In an anion deficient ferrite the principal process whereby pores shrink consists of the diffusion of anion

vacancies to the grain boundaries. In cation difficient ferrites on the other hand pores can be pulled along the grain boundries, coalesing with the other pores when they meet or come very close to them by involving oxygen transport via the gas phase, and the cation vacancies throughout the material surrounding the pore. The cation diffusion is facilitated by cation vacancies.

2.4 (d) Hot Pressing :

Ferrites have been fabricated to very high densities by hot pressing at relatively low temperatures. The powder is enclosed in a flexible container of rubber or plastic which may be evacuated and is compacted by immersing the container in an oil bath to which pressure is applied. The method also encourages continuous grain growth and favours to obtain low porosity and small grain size. It seems apparent that pressure should lead to a high degree of compaction and enhance contact between grains during sintring. At 1000°C ferrites have sufficient plasticity to flow a considerable extent at high pressures. It is favourable to produce high density compacts in which the original grain size is maintained. The composition containing volatile elements like Zn, Li benefit particularly when sealed containers are used, the net composition must be maintained, although the volatility may be associated with phase segregation.

2.5 PREPARATION OF FERRITE SAMPLES :

2.5 (a) Preparation :

Ferrite samples were prepared by usual ceramic method starting with the metal oxides. The general formula of the ferrite sample is

$Mg_{1+t}Ti_tFe_{2-2t}O_4$, where t = 0, .1, .2, .3, .4, .5. The method of preparation of the sample is as follow.

AR grade oxides MgO, Fe_2O_3 and TiO_2 were used for preparation The oxides were weighed in required mole proportions on a single pan balance and mixed thoroughly in an agate-morter with acetone. This mixture was then transferred into a platinum crucible and heated at 750°C for 8 hours. Then the samples were furnace cooled by switching off the furnace. The temperature of furnace was measured with the help of Cromel-Alumel thermocouple using digital multimeter. Thus pre-sintered samples were taken out from the crucibles. This hard samples were then ground in agate morter in acetone medium. Finally fine powder was collected in a clean glass tube.

2.5 (b) Pellet Formation :

Few grams of the sample was taken into agate mortar and wet mixture was done using P.V.A. as binder. Acetone was allowed to evaporate till the powder becomes completely dry. Then the dry powder was poured into the die having 1 cm diameter and cold pressed in a hydraulic press with the load of about 6-7 tonnes and load was left for 5 to 8 minutes. After removing the load pellet was taken out from the die.

2.5 (c) Final Sintering :

The pellets thus prepared were taken on a clean platinum foil and kept in furnace and sintered at 950°C for about 24 hours. They were then furnace cooled. The rate of cooling of the furnace was nearly 125°C/hour for first 2-3 hours and nearly 75°C/hour for the

intermediate stage droping to very low value asymptotically as the room temperature was approached within a span of about 10 hours.

For X-ray diffraction study the pellets were again ground and the fine powder is made. Some pellets were reserved for the use of resistivity measurement and magnetization study.

SECTION - B

X-RAY DIFFRACTION STUDY

2.6 INTRODUCTION :

The characterization of ferrites can be made by using the chemical analysis and mass spectrum analysis. The cation distribution can be studied from three types of studies (a) X-ray (b) neutron scattering and (c) the saturation magnetization measurements.

X-ray diffraction being an established tool to study solids. We have used the same tool with a view to confirm the formation of ferrite samples and characterization of crystal structure. In this section the brief theory of X-ray diffraction is given along with the principles of diffractometer.

2.7 CONDITION FOR X-RAY DIFFRACTION :

As the crystallites are randomly oriented, a reflection at the perticular position is due to a set of atomic planes satisfying Bragg's condition. The Braggs law is

$$n\lambda = 2d \sin\theta_{hkl} \qquad \ldots (2.5)$$

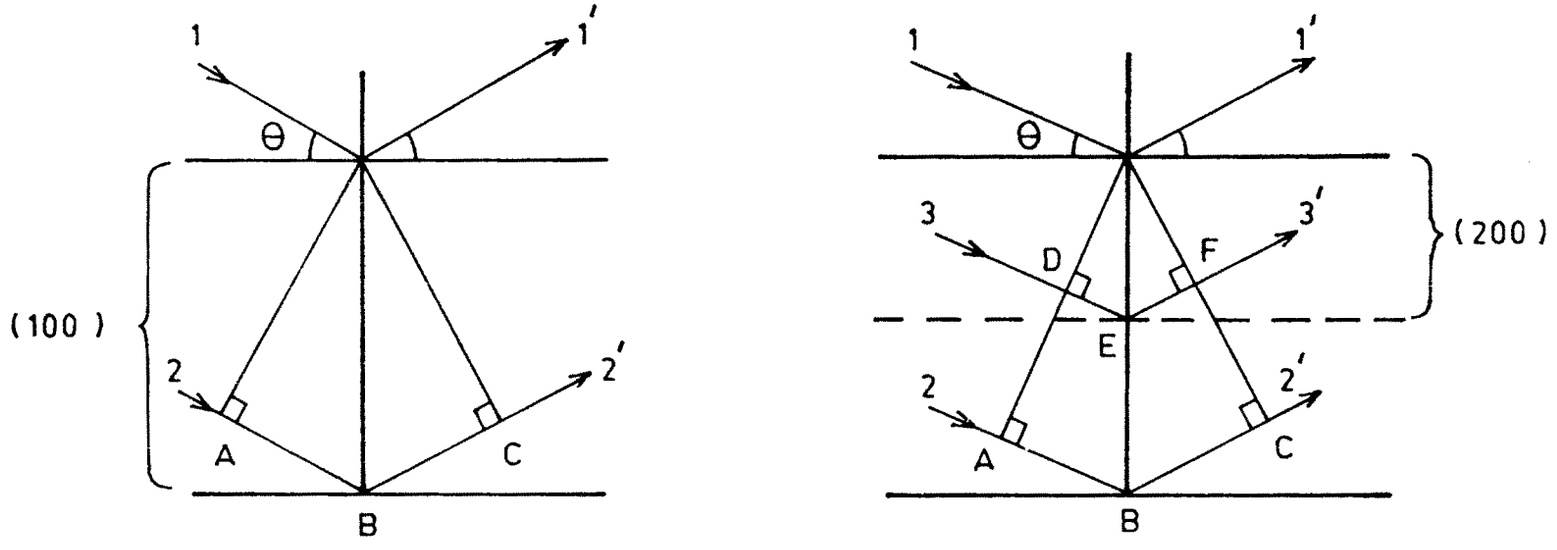

Fig. 2·2 - The application of Braggs law.

where,

d = the interplanar distance

n = the integral number

$$\theta < \text{Sin}\,\theta < 1 \Rightarrow n < 2d' \qquad \ldots (2.6)$$

since n = 1 is the least value of n in the diffraction condition for any observable angle 2 θ

$$N\lambda < 2d' \qquad \ldots (2.7)$$

Braggs law can be rearranged as

$$\lambda = 2\frac{d}{n}\,\text{Sin}\theta \qquad \ldots (2.8)$$

The coefficient of being unity, reflection of any order can be conveniently considered as the first order reflection from plane real or imaginary spaced at a distance 1/n of the previous spacing. For convenience replacing d'/n by d we get

$$\lambda = 2d\ \text{Sin}\,\theta \qquad \ldots (2.9)$$

The applicability of the law can be illustrated from fig.2.2. The number of whole wavelengths lying in the path difference between rays scattered by adjacent (hkl) plane is known as the order of diffracted beam. Fig. 2.2(a) represents the second order (100) reflection. If there is no real plane midway between the (100) plane it can be imagined as in fig. 2.2(b) forming first order reflection for adjacent (200) planes. In the same way (300), (400).. etc. reflction may be equivalent to the 3rd, 4th... etc. order from (100) plances respectively. Thus fourth order reflection from (hkl) planes of

spacing 'd' may be viewed as a first order reflection from (nh,nk,nl) planes of spacing d = $\frac{d'}{n}$. This suits with the definition of miller indices of planes parallel to the (hkl) planes with $\frac{1}{n}$ spacing of the latter.

The number of diffraction directions $2\theta_1$, $2\theta_2$, $2\theta_3$ ... etc. can be traced and photographed from the (100) planes by using a monocromatic incident beam at the angle θ_1, θ_2, θ_3 ... etc. which produce first, second, third etc. order of reflections respectively. The diffraction from other planes is also expected. The combination of Braggs law and plane-spacing expression of a particular crystal under investigation predict the diffraction angles for any set of planes.

$$\frac{1}{d} = \frac{h^2 + k^2 + l^2}{a^2} \qquad \ldots (2.10)$$

where 'a' denotes the unit cell size combining with the Braggs law, we have

$$\mathrm{Sin}^2\theta_{hkl} = \frac{\lambda^2}{4a^2}(h^2+k^2+l^2) \qquad \ldots (2.11)$$

The equation becomes representative of Braggs angles for diffra ction occuring from the plane (h,k,l) for known value of λ. The relation between 'd' and 'a' changes with change of crystal structure The details of the formula are given elsewhere.

2.8 X-RAY DIFFRACTOMETER AND ITS PRINCIPLE :

The principle and essential features of the diffractometer are shown in fig. 2.3. An incident beam of x-ray passing through a filter is collimated by the slit 'A'. The monocromatic radiation is thus

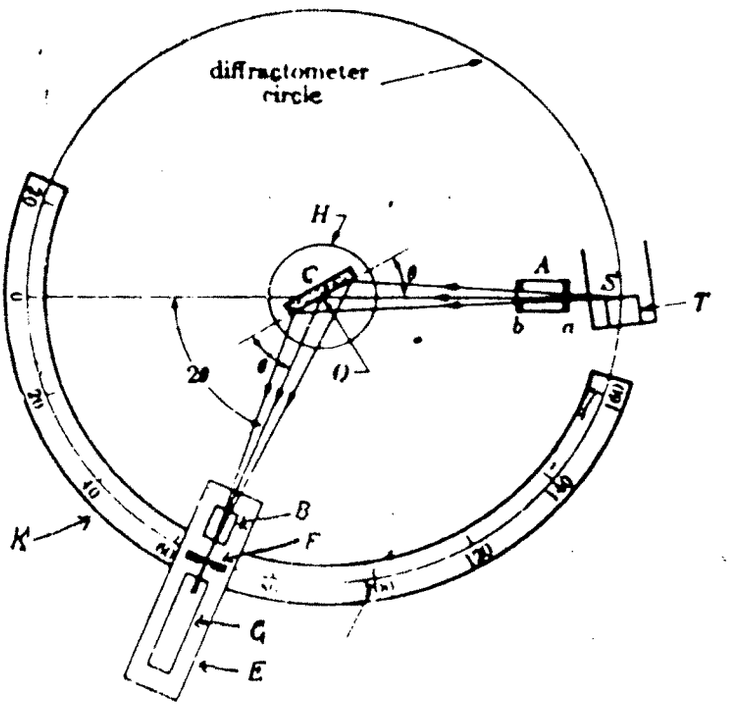

Fig. 2.3

incident on the specimen, kept on holder C and thus reflected by crystal planes satisfying Braggs law. As the crystallites are randomly oriented, a reflection at the particular position is due to a set of atomic planes satisfying Braggs condition. As a result a convergent beam diffracted by the set of parallel planes is produced which comes to a focus atslit 'F' and then enters the counter 'G'. B is a special slit which collimates the diffracted beam. The counter G is connected to a count rate meter and the output of the circuit is fed to a fast automatic recorder which registers counts per second versus '2θ'. The location of the centroid of the peak recorded gives $2\theta_{hkl}$ for the corresponding Bragg-reflection.

The receiving slits and the counter are supported on the carriage 'E' which can be rotated about the vertical axis through 'C' and whose angular position 2θ can be read on the graduated circular scale 'K'. As the counter G moves through 2θ degrees, through mechanical coupling between E and H, which ensures that the complementary angles of incidance and reflection from the flat specimen are always equal to each other, the counter presents itself to receive the focussed beam diffracted at a glancing angle of θ. The counter is power driven at a constant angular velocity about the axis of diffractometer for any desired angular range 1° to 160°. The other advantage of the diffractometer over the Debye-Scherrer method is that it gives a quantitative measure of the intensity.

In the present work PW 1700 automated X-ray powder diffractometry system was used. All the work was carried out at Regional Sophisticated Instrumentation Centre, Nagpur.

2.9 INDEXING OF THE POWDER PATTERN :

The diffractograms of the system

$$Mg_{1+t}Ti_tFe_{2-2t}O_4 \quad (0 < t < 0.5)$$

were obtained with diffractometer. The object of scanning was kept to cover as wide range of 2θ as possible between 0° to 100°. The value of $\sin 2\theta$ was calculated for each peak observed in the pattern. The set of the $\sin 2\theta$ values is the raw material for the determination of cell size and shape.

For cubic lattice the relation between the interplanar distance 'd_{hkl}', lattice parameter 'a' and the indices 'hkl' can be represented by the formula

$$d_{hkl} = \frac{a}{h^2+k^2+l^2} \qquad \ldots (2.14)$$

As the peak in the diffraction pattern is obtained, the Braggs law must be obeyed,

$$2\, d_{hkl}\, \mathrm{Sin}\theta_{hkl} = \lambda \qquad \ldots (2.15)$$

Combining these two equations,

$$2 \left(\frac{a}{h^2+k^2+l^2} \right) \mathrm{Sin}\,\theta_{hkl} = \lambda$$

$$\frac{\mathrm{Sin}^2\theta_{hkl}}{h^2+k^2+l^2)} = \frac{\mathrm{Sin}^2\theta_{hkl}}{S} = \frac{2}{4a^2} \qquad \ldots (2.16)$$

Where the sum, $S = h^2+k^2+l^2$

The sum 'S' is always an integer and the value of $\frac{\lambda^2}{4a^2}$ must be constant for any observed peak in the pattern. Thus the set of integers 'S' should be selected properly to yield a constant quotient

when divided by one into the observed $Sin^2\theta$ values. Rearranging the equation (2.16)

$$Sin^2\theta_{hkl} = \frac{\lambda^2 S}{4a^2} \qquad \ldots (2.17)$$

We find that the quantity $\frac{\lambda^2}{4a^2}$ is the greatest common factor (GCE) in $Sin^2\theta$. As first step GCF was determined from a few lines at the lower angles and then all the other proper integers were found Once the integers 'S' were known the indices 'hkl' of reflecting plane were written down by inspection. If the set of integers satisfying equation (2.16) for cubic system were not found, then other possible system can be checked.

2.10 RESULTS AND DISCUSSIONS :

From the tables (2.1 to 2.6) it is observed that all the samples show the spinel structure and they form complete solid solution. The planes agree well with those of the spinel structure. The lattice constant for pure $MgFe_2O_4$ agrees well with the reported value Additional phases have been observed in the sample with t = 0.4 & t = 0.5. These lines have been identified to be of TiO_2 phases.

In fig. 2.a-f diffractograms of the samples are given. The observed and calculated values and (hkl) planes are given in table 2.1 to 2.6.

From Fig. 2.4 variation of lattice parameter with containt of Ti^{4+} is shown for the system $Mg_{1+t}Ti_tFe_{2-2t}O_4$ (t = 0,0.1,0.2,0.3,0.4, 0.5). No definite trend is observed by the compositional variation

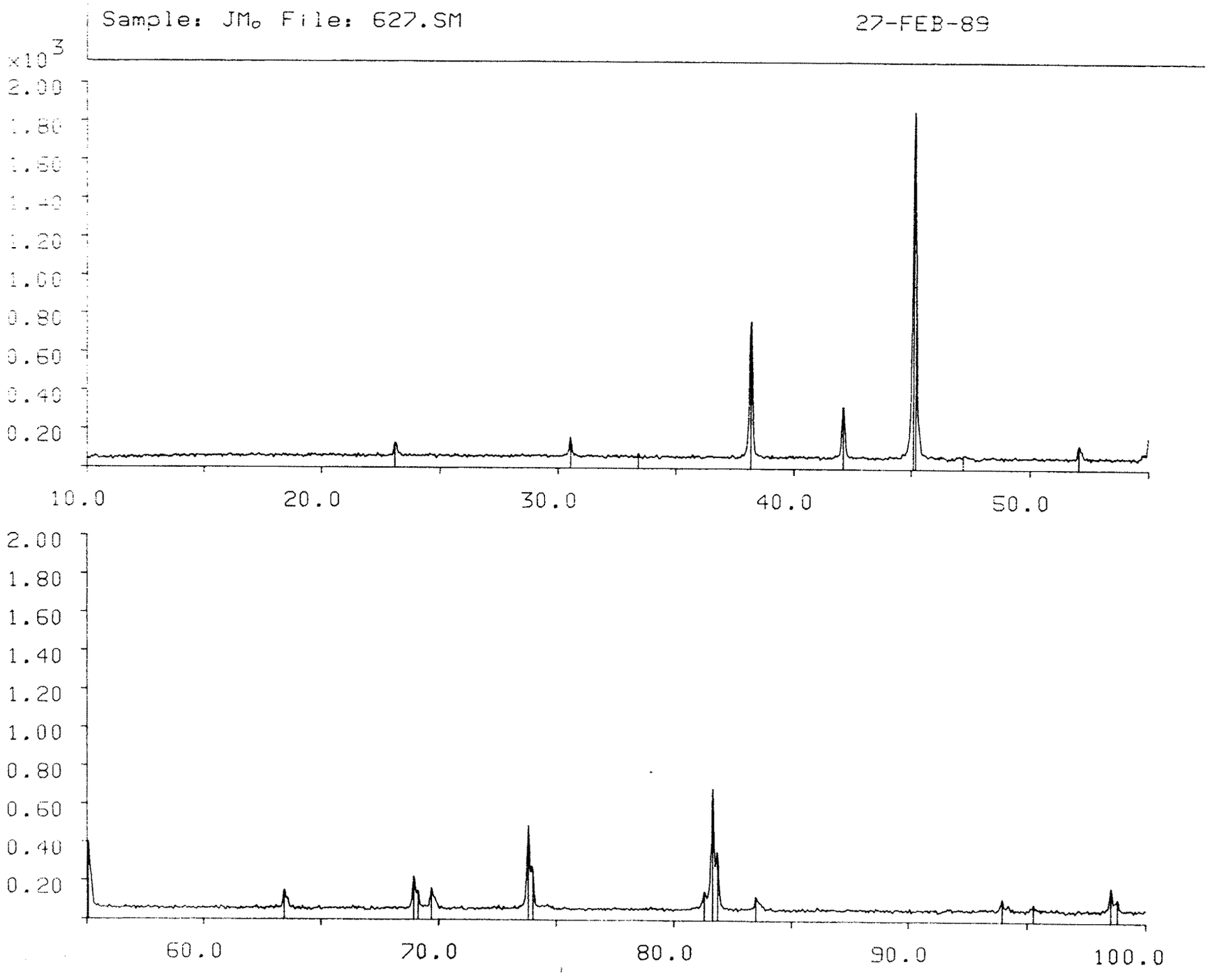
Sample: JM6 File: 627.SM
27-FEB-89
x10 3
2.00
1.80
1.60
1.40
1.20
1.00
0.80
0.60
0.40
0.20
10.0
20.0
30.0
40.0
50.0
2.00
1.80
1.60
1.40
1.20
1.00
0.80
0.60
0.40
0.20
60.0
70.0
80.0
90.0
100.0

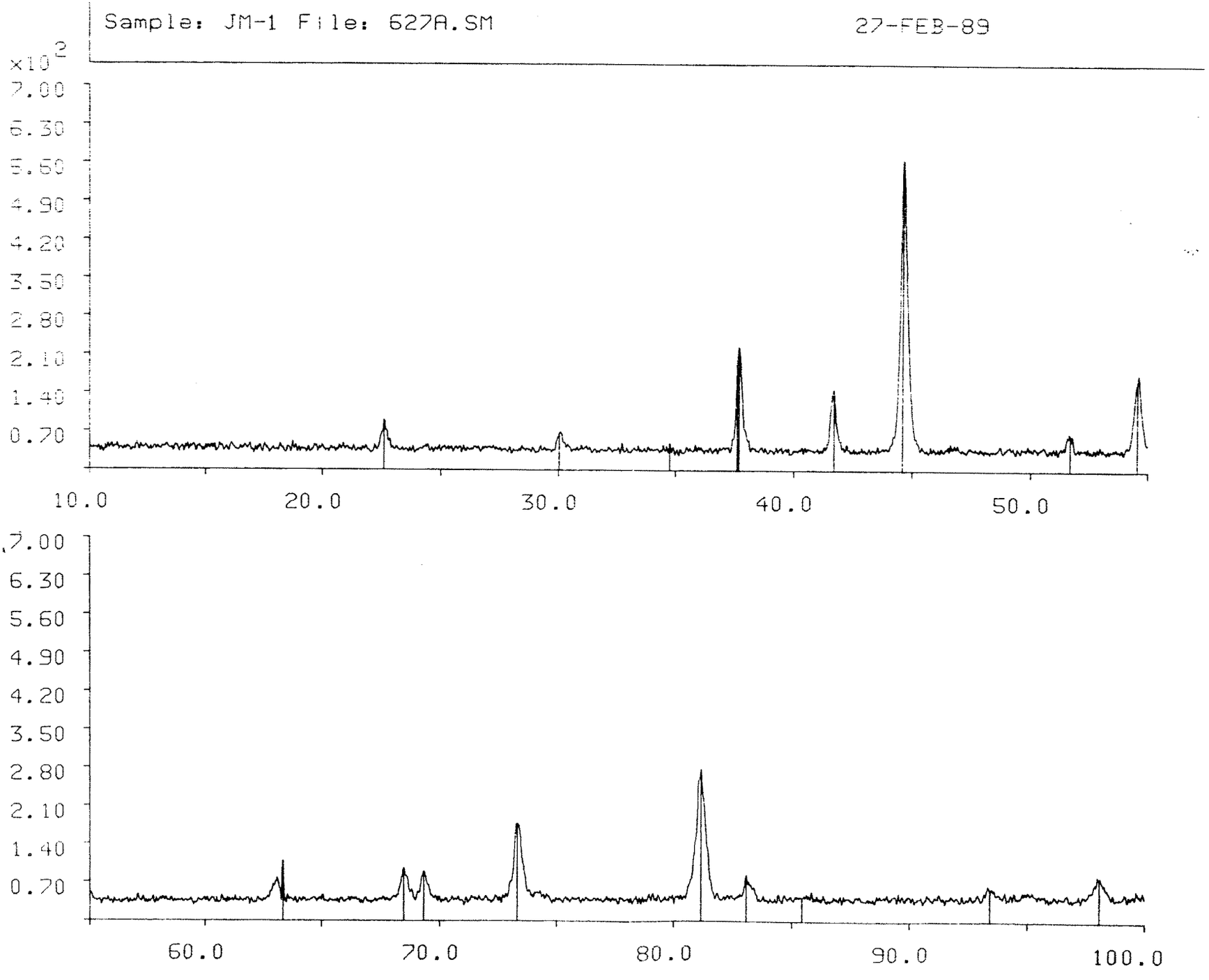
Sample: JM-1 File: 627A.SM
27-FEB-89
x10 2
7.00
6.30
5.60
4.90
4.20
3.50
2.80
2.10
1.40
0.70
10.0
20.0
30.0
40.0
50.0
7.00
6.30
5.60
4.90
4.20
3.50
2.80
2.10
1.40
0.70
60.0
70.0
80.0
90.0
100.0

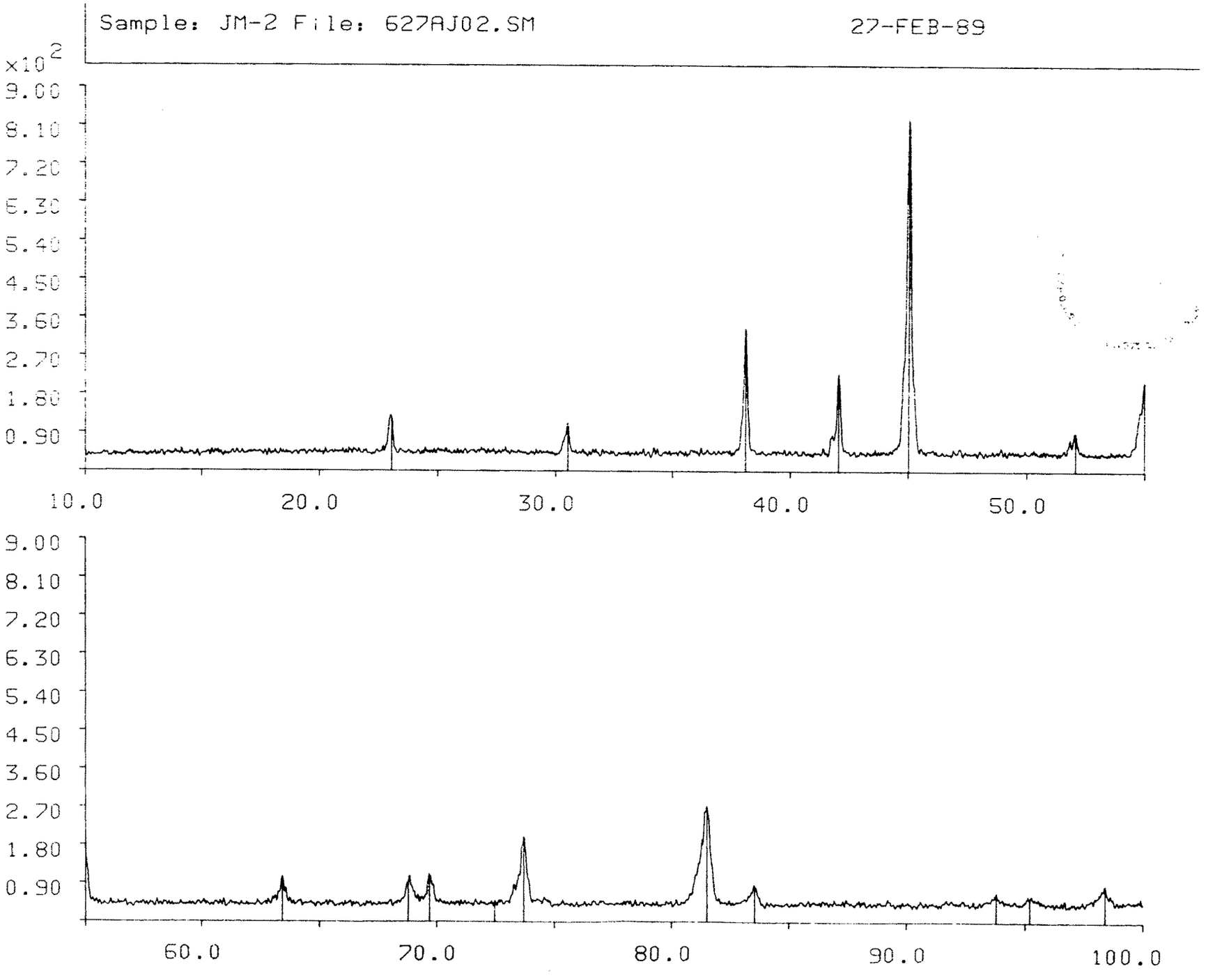
Sample: JM-2 File: 627AJ02.SM
27-FEB-89
x10 2
9.00
8.10
7.20
6.30
5.40
4.50
3.60
2.70
1.80
0.90
10.0
20.0
30.0
40.0
50.0
9.00
8.10
7.20
6.30
5.40
4.50
3.60
2.70
1.80
0.90
60.0
70.0
80.0
90.0
100.0

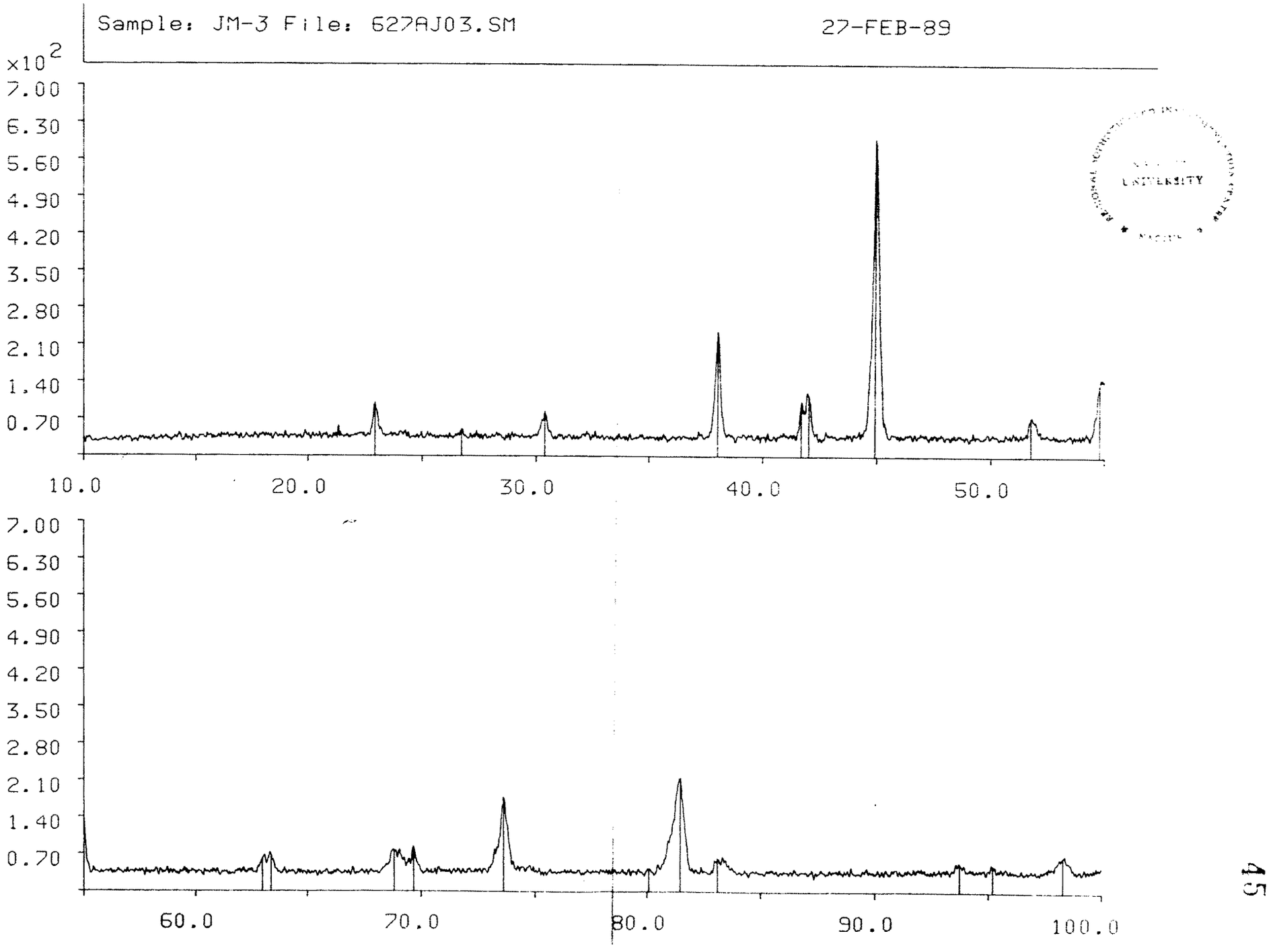
Sample: JM-3 File: 627AJ03.SM
27-FEB-89
x10 2
7.00
6.30
5.60
4.90
4.20
3.50
2.80
2.10
1.40
0.70
10.0
20.0
30.0
40.0
50.0
60.0
70.0
80.0
90.0
100.0

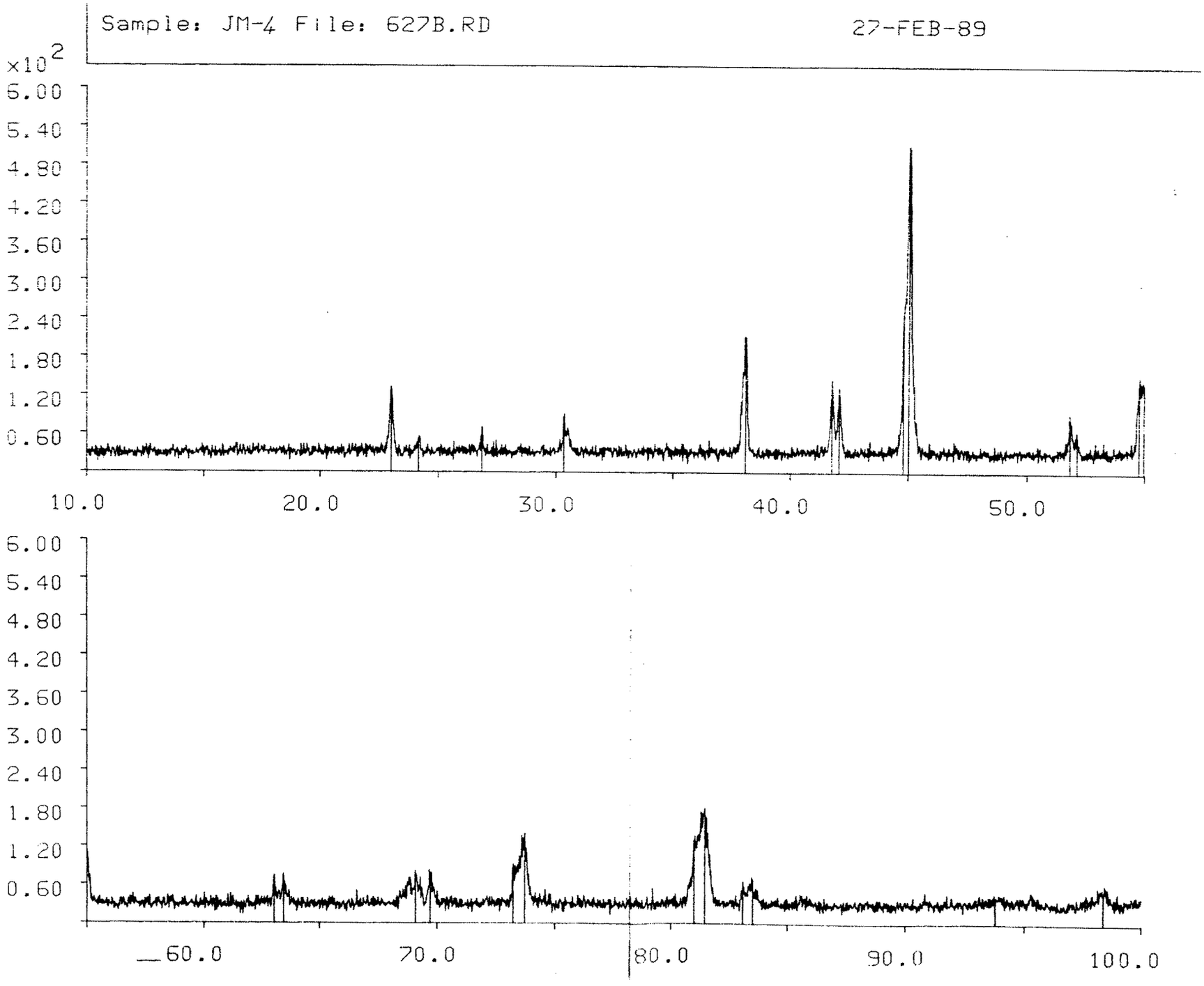
Sample: JM-4 File: 627B.RD
27-FEB-89
x10 2
6.00
5.40
4.80
4.20
3.60
3.00
2.40
1.80
1.20
0.60
10.0
20.0
30.0
40.0
50.0
6.00
5.40
4.80
4.20
3.60
3.00
2.40
1.80
1.20
0.60
60.0
70.0
80.0
90.0
100.0

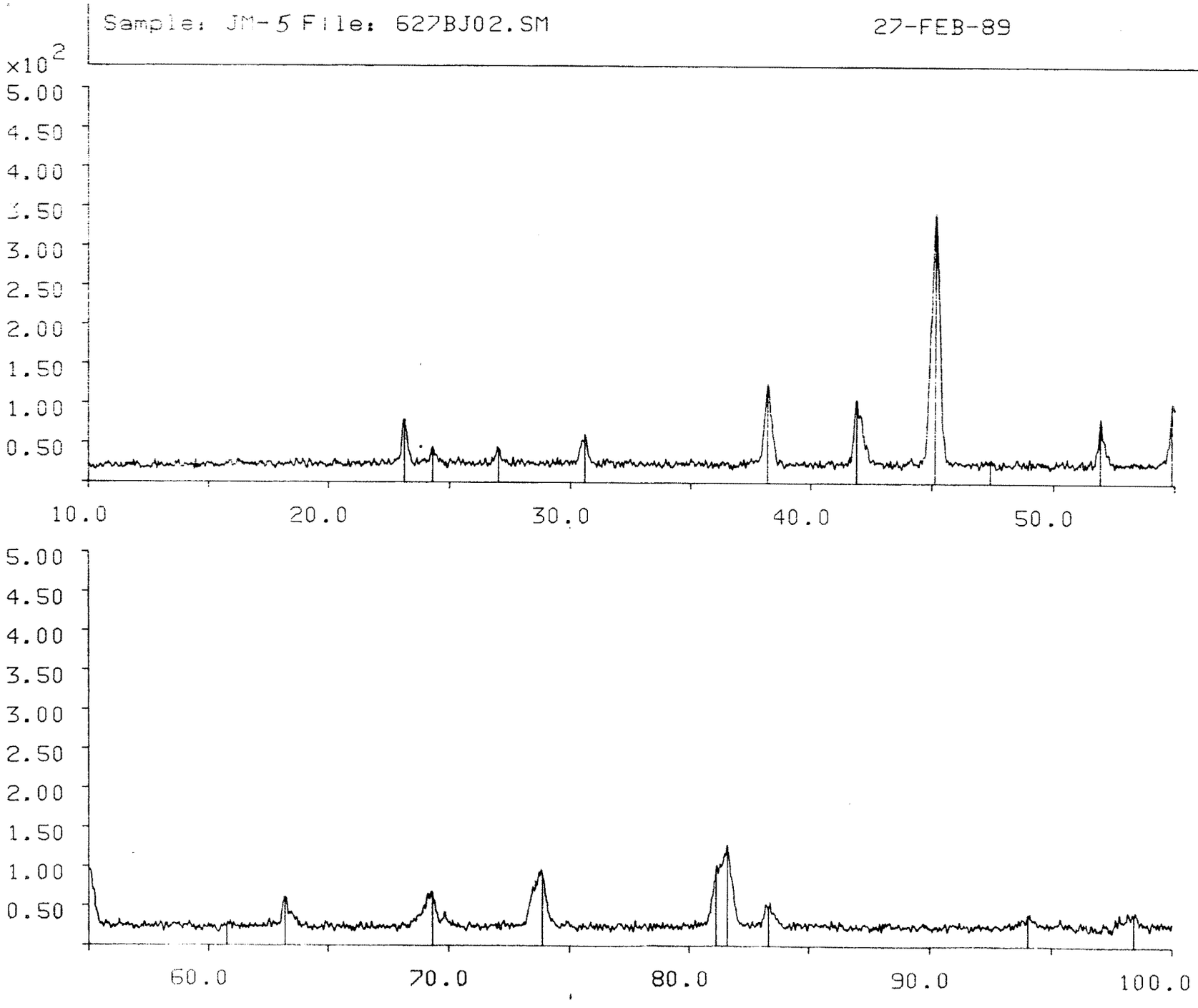
Sample: JM-5 File: 627BJ02.SM
27-FEB-89
x10 2
5.00
4.50
4.00
3.50
3.00
2.50
2.00
1.50
1.00
0.50
10.0
20.0
30.0
40.0
50.0
5.00
4.50
4.00
3.50
3.00
2.50
2.00
1.50
1.00
0.50
60.0
70.0
80.0
90.0
100.0

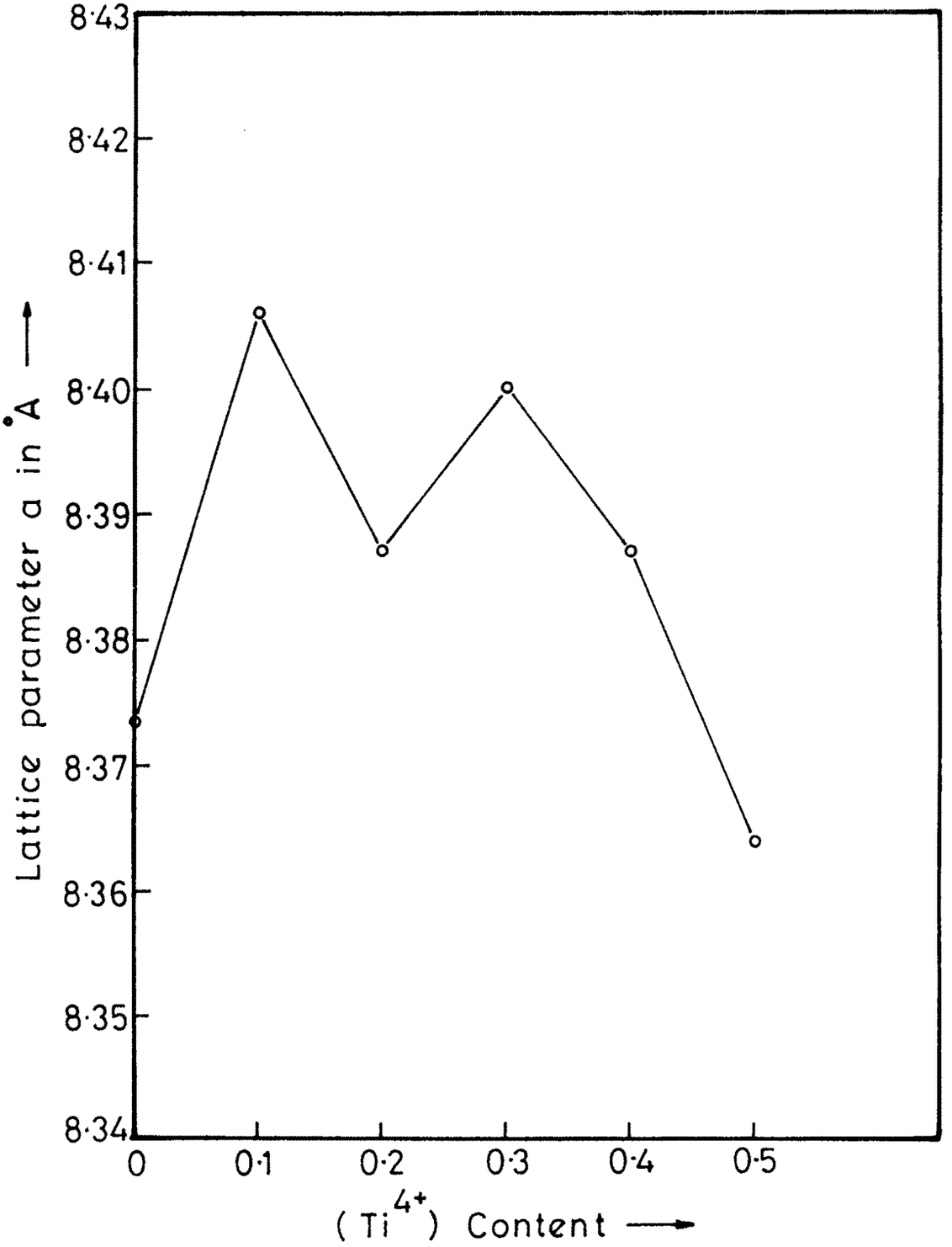
8·43
8·42
8·41
8·40
8·39
8·38
8·37
8·36
8·35
8·34
Lattice parameter a in Å
0
0·1
0·2
0·3
0·4
0·5
(Ti4+) Content

Fig. 2·4

X-Ray Powder Diffraction from $Mg_{1+t}Ti_tFe_{2-2t}O_4$

Table : 2.1

t = 0 $MgFe_2O_4$

hkl	observed d	calculated d
111	4.8332	4.8140
220	2.9598	2.9606
311	2.5248	2.5248
400	2.0940	2.0935
422	1.7100	1.7093
511	1.6120	1.6115
440	1.4809	1.4803
620	1.3242	1.3240
533	1.2776	1.2770

Table : 2.2

t = 0.1 $Mg_{1.1}Ti_{0.1}Fe_{1.8}O_4$

hkl	observed d	calculated d
111	4.9413	4.8858
220	3.0030	2.9919
311	2.5515	2.5515
400	2.1118	2.1156
422	1.8430	1.8923
511	1.6213	1.6286
440	1.4882	1.4959
620	1.3301	1.3380
533	1.2819	1.2905

X-Ray Powder Diffraction from $Mg_{1+t}Ti_tFe_{2-2t}O_4$

Table : 2.3

t = 0.2 $Mg_{1.2}Ti_{0.2}Fe_{1.6}O_4$

hkl	observed d	calculated d
111	4.8445	4.8425
220	2.9664	2.9653
311	2.5289	2.5289
400	2.0971	2.09685
422	1.7129	1.7120
511	1.6140	1.6142
440	1.4830	1.4827
620	1.3261	1.3261
533	1.2790	1.2791

Table : 2.4

t = 0.3 $Mg_{1.3}Ti_{0.3}Fe_{1.4}O_4$

hkl	observed d	calculated d
111	4.8664	4.8507
220	2.9711	2.9704
311	2.5332	2.5332
400	2.1008	2.10043
422	1.7125	1.7149
511	1.6157	1.6169
440	-	-
620	1.3265	1.3284
533	1.2797	1.2812

X-Ray Powder Diffraction from $Mg_{1+t}Ti_tFe_{2-2t}O_4$

Table : 2.5

t = 0.4 $Mg_{1.4}Ti_{0.4}Fe_{1.2}O_4$

hkl	observed d	calculated d
111	4.8502	4.8425
220	2.9649	2.9654
311	2.5289	2.5289
400	2.1023	2.09685
422	1.7067	1.7121
511	1.6137	1.6142
440	1.4837	1.4827
620	1.3261	1.3262
533	1.2790	1.2791

Table : 2.6

t = 0.5 $Mg_{1.5}Ti_{0.5}FeO_4$

hkl	observed d	calculated d
111	4.8265	4.8294
220	2.9585	2.9574
311	2.5221	2.5221
400	2.1009	2.0912
422	1.7015	1.7075
511	1.6106	2.6098
440	1.4886	1.4787
620	1.3232	1.3226
533	1.2787	1.2756

of lattice parameter. However, except for the sample corresponding to t = 0.5 the lattice parameter for all samples is greater than that for $MgFe_2O_4$. In table 2.7 the ionic radii of the cations involved are given.[14]

Table 2.7

Ions	Mg^{2+}	Fe^{3+}	Ti^{4+}
Ionic radii	0.75°A	0.67°A	0.68°A

In our system where Ti^{4+} ions are substituted by amount 't'. The Fe^{3+} ion concentration decreases by the amount (2-2t), while the Mg^{2+} ion concentration increases by the amount (1+t). Thus as both Mg^{2+} and Ti^{4+} have ionic volumes greater than that for Fe^{3+}. All the samples exhibits large values of lattice parameter when Fe^{3+} ions replaced by Ti^{4+} ions. A.R.Das et.al.[15] have studied the variation of lattice parameter and magnetization in Ni-Zn ferrites on substituting Ti^{4+} and Zr^{4+} and Sn^{4+}. They observed that addition of both Ti^{4+} and Zr^{4+} initially reduces the lattice parameter while afterward the lattice parameter goes on increasing the content of Ti^{4+} and Zr^{4+}. They have explained the initial fall in the lattice parameter by the combined effect of the cation size on b, the repulsion parameter and of the A-site charge[16] on M the Madelung constant, where the lattice parameter is proportional to $(b/M)^{1/9}$. The entry of four and higher valancy cations in A site increases their charge, resulting in an increase in 'M'. When the the substituting ions are small like Ti^{4+} (b/M) decreases. The

lattice parameter falls initially and after the minimum point, Ti^{4+} ions enter on B-site resulting in reduction of charge in A, a fall in 'M' and an increase in (b/M).

In the system $Mg_{1+t}Ti_tFe_{2-2t}O_4$ the general formula for cation distribution may be given by,

$$(Fe_{1-x-y}Mg_xTi_y)\ [Fe_{1+x+y-2t}Mg_{1+t-x}Ti_{t-y}]O_4$$

in which the cation enclosed by ( ) occupy in A-site while those enclosed by [ ] occupy the B-site. However, there is evidance that the value of 'y' is small[17] as the result of the maximum charge neutralization. In other words, the tetrahedral Fe^{3+} ions are mainly replaced by Mg^{2+} ions and octahedral Fe^{3+} ions are replaced by Ti^{4+} ions. Therefore it is reasonable to consider the cation distribution to be of the form,

$$(\ Fe^{3+}_{1-x}Mg^{2+}_x\ )\ [Fe^{3+=}_{1+x-2t}Mg^{2+}_{1+t-x}Ti^{4+}_t\ ]\ O_4$$

On the basis of existing predictions[18,19,20] the preferred site for Ti, Sn, Nb and Ni are B-site and that for Zn is A-site. A number of workers had postulated movement of ions to the non-preferred sites i.e. Zn^{2+} to B-site,[21] Sn^{4+} to A-site[19] and Ti^{4+} to A-site[18] in order to explain observed variation in properties and x-ray intensity study.[21] Hence to understand the compositional variation of lattice parameter exactly will required precise determination of cation distribution. In Fig. 2.5 compositional variation of bond lengths r_A and r_B is shown r_A and r_B values were evaluated using the ratio

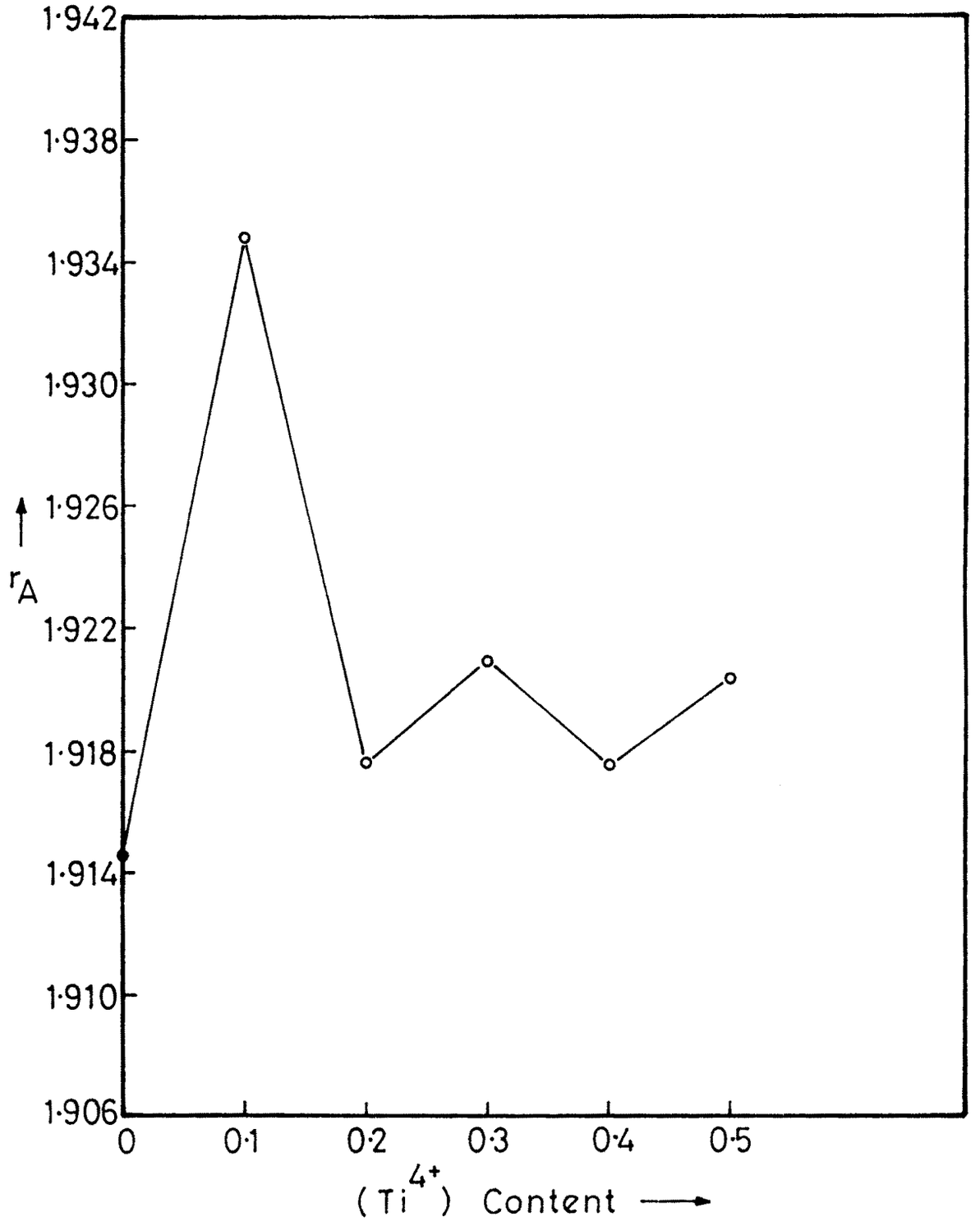
1·942
1·938
1·934
1·930
1·926
1·922
1·918
1·914
1·910
1·906
r_A
0
0·1
0·2
0·3
0·4
0·5
(Ti^{4+}) Content

Fig. 2·5 (a)

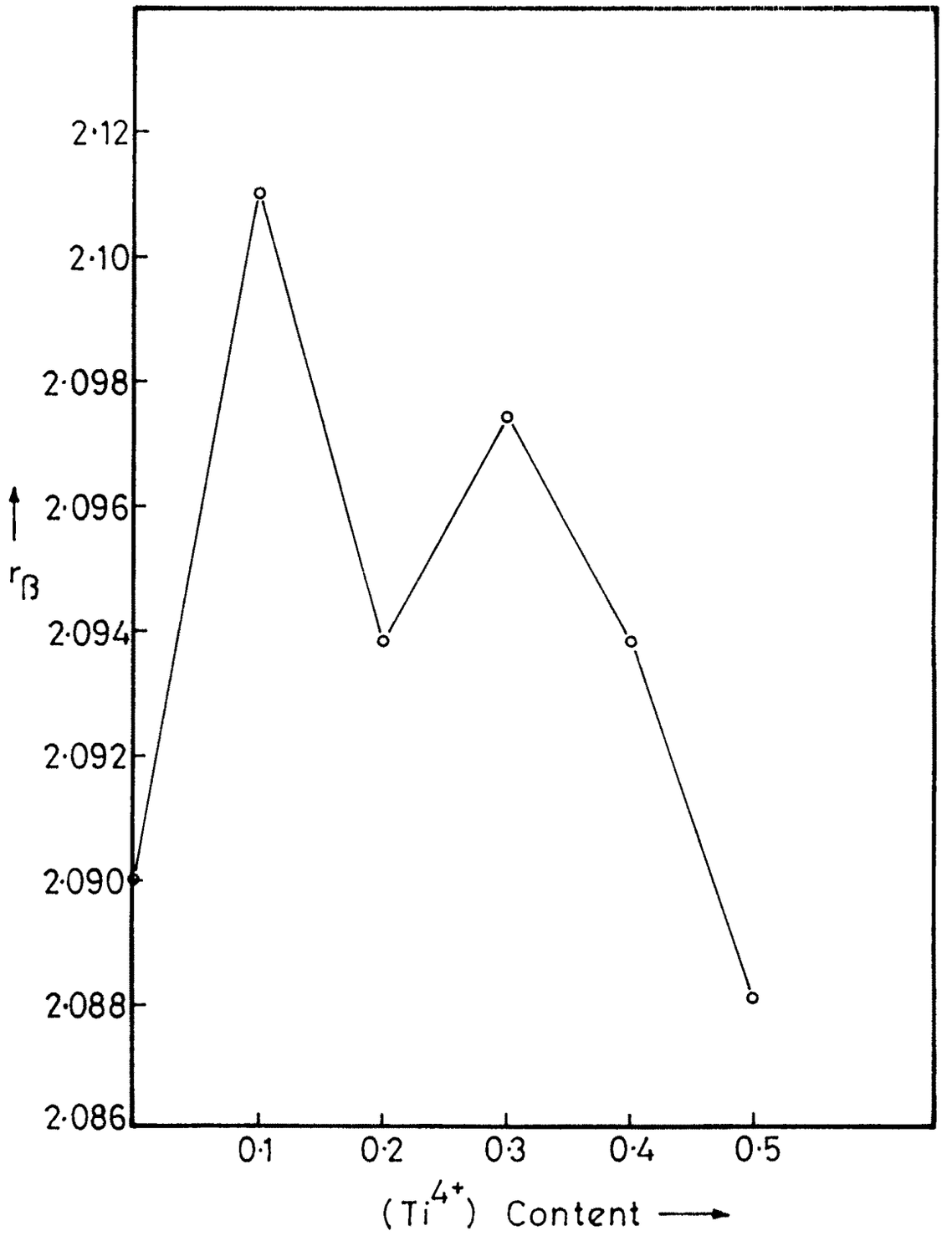
2·12
2·10
2·098
2·096
2·094
2·092
2·090
2·088
2·086
r_β
0·1
0·2
0·3
0·4
0·5
(Ti^{4+}) Content

Fig. 2·5 (b)

$$r_A = a\sqrt{3}\,(\delta + \frac{1}{8})$$

$$r_B = a\,(3\delta^2 - \frac{1}{2}\delta + \frac{1}{16})^{\frac{1}{2}}$$

where $= u - 0.37$

The 'u' values were taken from the data reported earlier[22]. From both the figures it is seen that both r_A and r_B values of all the samples are greater than that for 'Mg'-ferrite, while r_B values for all the samples except for the sample corresponding to $1 = 0.5$ are also greater than that for Mg-ferrite. Levine's work on bond susceptibility in spinel[23] showed an inverse relationship between the covalent character of the spinel and the bond length.

Thus it can be concluded that addition of Ti^{4+} has an effect of decreasing the iono-covalent character of the ferrite.

REFERENCES

1. Hirota E., Jap. J. Appl. Phys. 5, 1125 (1966).
2. Standley K.J., 'Oxide Magnetic Materials', Clarendon Press, Oxford (1972).
3. Swallow D., Jordon A.K., Proc. Brit. Ceram Soc. 2, 1 (1964).
4. Clobe R.L., Burke J.E., Progress in ceramic Sci. Vol.III, p. 197 (1963).
5. Stuijts A.L., Kooy C., Sci. Ceram. 2, 231 (1965).
6. Nabarro F.R.N. Rept. Conf. Strength of Solids Phys. Soc., London p. 75 (1948).
7. Herring C., J. Appl. Phys. 21, 437 (1950).
8. Burke J.E. in kinetics of high temperature processes Ed. W.D.Kingery N.Y. p. 109 (1959).
9. Zener C. See Smith C.S. Trans AIME 175, 15 (1948).
10. Paulus M., Ferrites Proc. Int. Conf. Tokyo p.115 (1970).
11. Stuijts A.L. Proc. Brit. Ceram. Soc. 2, 73 (1964).
12. Reignen P.J.L. Science of Ceramics 4, 169 (1968).
13. Cullity B.D. 'Elements of x-ray diffraction' Addision Wesley Publishing Co. INC. England (1959).
14. Standley K.J. 'Oxide Magnetic Materials' Clarendon Press Oxford p. 28 (1972).
15. Das A.R., Ananthan V.S. and Khan D.C., J. Appl. Phys. 57 (1) p. 4189 (1985).
16. Khan D.C., Misra M. and Das A.R., J. Appl. Phys. 53 p.2722 (1982).

17. Verwey E.J.W. and Heilman E.L., J. Chem. Phys. 15, 673 (1957).

18. Gorter E.W., Philips Res. Rep. 29, 93 (1974).

19. Puri R.K. and Varshney Usha, J. Phys. Chem. Solids 44, 655 (1983).

20. Blass G., Philips Res. Rep. 18, 400 (1963).

21. Miyahara Y. and Sai F., J. Phys. Soc. Jpn. 41, 1522 (1976).

22. Standley K.I. "Oxide Magnetic Materials" Clarendon Press Oxford p. 24 (1972).

23. Levine B.F., Phys. Rev. B-7, 2591 (1975).